© 2018. Published by The Company of Biologists Ltd | Journal of Cell Science (2018) 131, jcs213272. doi:10.1242/jcs.213272

RESEARCH ARTICLE

TMEM55a localizes to macrophage phagosomes to downregulate phagocytosis

Shin Morioka[1], Kiyomi Nigorikawa[1], Eri Okada[1], Yoshimasa Tanaka[1], Yoshihiro Kasuu[1], Miho Yamada[1], Satoshi Kofuji[1], Shunsuke Takasuga[2], Hiroki Nakanishi[3], Takehiko Sasaki[2] and Kaoru Hazeki[1,*]

ABSTRACT

TMEM55a (also known as PIP4P2) is an enzyme that dephosphorylates the phosphatidylinositol (PtdIns) PtdIns(4,5)P_2 to form PtdIns(5)P *in vitro*. However, the *in vivo* conversion of the polyphosphoinositide into PtdIns(5)P by the phosphatase has not yet been demonstrated, and the role of TMEM55a remains poorly understood. Here, we found that mouse macrophages (Raw264.7) deficient in TMEM55a showed an increased engulfment of large particles without affecting the phagocytosis of *Escherichia coli*. Transfection of a bacterial phosphatase with similar substrate specificity to TMEM55a, namely IpgD, into Raw264.7 cells inhibited the engulfment of IgG-erythrocytes in a manner dependent on its phosphatase activity. In contrast, cells transfected with PIP4K2a, which catalyzes PtdIns(4,5)P_2 production from PtdIns(5)P, increased phagocytosis. Fluorescent TMEM55a transfected into Raw264.7 cells was found to mostly localize to the phagosome. The accumulation of PtdIns(4,5)P_2, PtdIns(3,4,5)P_3 and F-actin on the phagocytic cup was increased in TMEM55a-deficient cells, as monitored by live-cell imaging. Phagosomal PtdIns(5)P was decreased in the knockdown cells, but the augmentation of phagocytosis in these cells was unaffected by the exogenous addition of PtdIns(5)P. Taken together, these results suggest that TMEM55a negatively regulates the phagocytosis of large particles by reducing phagosomal PtdIns(4,5)P_2 accumulation during cup formation.

KEY WORDS: Phosphatidylinositol(4,5)-bisphosphate 4-phosphatase, Phagocytosis, Macrophage, TMEM55a, F-actin, IpgD

INTRODUCTION

Phagocytosis by professional phagocytes is central for the elimination of microbial pathogens, innate and adaptive immunity, and clearance of apoptotic cells and debris. Although the precise mechanisms involved in phagocytosis vary depending on receptors involved or target particle sizes, they share the common feature of regulation through phosphoinositide derivatives. For example, F-actin assembly accelerated by PtdIns(4,5)P_2 facilitates the extension of pseudopods, which are indispensable for the initial capture of phagocytic targets regardless of the target species (Botelho et al., 2000; Freeman and Grinstein, 2014; Szymańska et al., 2008). However, the following phase, closure of the phagocytic cup, proceeds via different mechanisms between large (>5 µm) and small targets. Phagosomal accumulation of PtdIns(3,4,5)P_3, as catalyzed by the class I phosphoinositide 3-kinase (PI3K)-induced phosphorylation of PtdIns(4,5)P_2, is essential for the ingestion of large particles but is dispensable for the uptake of smaller targets (Araki et al., 1996; Cox et al., 1999; Schlam et al., 2015). The PI3K product functions to recruit Rho GTPase-activating proteins (RhoGAPs) to the phagocytic cup, which are then responsible for the inactivation of Rho family GTPases and the termination of actin assembly (Schlam et al., 2015). This coordinated disassembly of F-actin is required for the closure of the large phagocytic cup (Ikeda et al., 2017).

TMEM55a and TMEM55b, also known as type II (PIP4P2) and type I (PIP4P1) PtdIns(4,5)P_2 4-phosphatase, respectively, were first identified as enzymes that catalyze the hydrolysis of PtdIns(4,5)P_2, but no other phosphoinositides, resulting in the generation of PtdIns(5)P (Ungewickell et al., 2005). Their enzymatic activities and substrate specificities have been determined *in vitro*, but the *in vivo* conversion of the polyphosphoinositide into PtdIns(5)P by the phosphatase has not yet been demonstrated and their roles have mostly been inferred from overexpression studies. Since the product of the phosphatase, PtdIns(5)P, predominantly exists in the nucleus and interacts with the plant homodomain (PHD) finger of inhibitor of growth protein-2 (ING2), it is suggested that TMEM55b (type I) generates nuclear PtdIns(5)P, which is responsible for activation of p53 (also known as TP53) and the resultant increase of apoptosis (Zou et al., 2007). However, when transfected in HeLa cells, both TMEM55a and TMEM55b are localized to late endosomal or lysosomal membrane, so it is likely that the phosphatases also play roles in the endosome (Ungewickell et al., 2005). Upon overexpression of these proteins in HEK293 cells, the degradation of EGF receptor following ligand binding is accelerated (Ungewickell et al., 2005). Accordingly, it was speculated that TMEM55a and TMEM55b are involved in the lysosomal degradation of plasma membrane receptors. However, ectopic expression of the virulence factor IpgD, a phosphatase with similar substrate specificity to that of TMEMs (Niebuhr et al., 2002), causes a delay in EGF receptor degradation (Boal et al., 2015; Ramel et al., 2011). Thus, the physiological role of the PtdIns(4,5)P_2 4-phosphatases remains obscure.

In this paper, to investigate the physiological role of TMEM55a, we prepared Raw264.7 macrophages deficient in TMEM55a by using specific shRNA methodology. These cells possessed enhanced phagocytic activity against two distinct large particles, sheep red blood cells (RBCs) with membrane-bound IgG (hereafter IgG-RBCs) and zymosan, without affecting *Escherichia coli* phagocytosis. The accumulation of PtdIns(4,5)P_2 was increased, whereas the product of TMEM55a, PtdIns(5)P, was decreased on phagocytic cups in these cells, suggesting that TMEM55a dephosphorylates PtdIns(4,5)P_2 to PtdIns(5)P on phagosomes.

[1]Graduate School of Biomedical & Health Sciences, Hiroshima University, Hiroshima 734-8553, Japan. [2]Department of Pathology and Immunology, Akita University School of Medicine, Akita 010-8543, Japan. [3]Research Center for Biosignal, Akita University School of Medicine, Akita 010-8543, Japan.

*Author for correspondence (khazeki@hiroshima-u.ac.jp)

K.N., 0000-0002-4285-9695; K.H., 0000-0001-8087-0337

Received 14 November 2017; Accepted 22 January 2018

Journal of Cell Science (2018) 131, jcs213272. doi:10.1242/jcs.213272

This hypothesis was supported by the observation that fluorescent protein-tagged TMEM55a transfected in macrophages localizes to phagosomes during phagocytosis. The increased PtdIns(4,5)P_2 is likely immediately phosphorylated to PtdIns(3,4,5)P_3 by class I PI3K, because PtdIns(3,4,5)P_3 was also increased on phagocytic cups of TMEM55a-deficient cells. The augmentation of PtdIns(3,4,5)P_3 in addition to PtdIns(4,5)P_2 may thus be responsible for the target size-dependent activation of phagocytosis in the TMEM55a-knockdown cells.

RESULTS

Preparation of cells deficient in TMEM55a or TMEM55b

To investigate the role of endogenous TMEM55a and TMEM55b, we generated RAW264.7 cells expressing shRNA directed against these phosphatases. Two cell lines (229 and 322 in Fig. 1A and Table S1) that produce shRNAs against distinct TMEM55a sequences (shTMEM55a) were prepared. The mRNA was reduced to 20% and 40% of that in control cells in the shTMEM55a-expressing lines 229 and 322, respectively (Fig. 1A). TMEM55b mRNA in the cells expressing shRNA against TMEM55b (shTMEM55b) (Table S1) decreased to 20% of that in control cells (Fig. 1B). We tried to estimate the endogenous expression of the TMEM55 proteins in the knockdown cells, but the antibodies from a commercial source did not work. To determine the knockdown efficiency, the knockdown cells were transfected with FLAG-tagged TMEM55a or TMEM55b and the expression was determined with anti-FLAG antibody. A large quantity of FLAG–TMEM55b protein was expressed in the control cells as well as shTMEM55a cells, but did not express in TMEM55b-knockdown cells (Fig. 1C, middle panel). The expression of FLAG–TMEM55a was far smaller than that of FLAG–TMEM55b but was detectable in a longer exposure (Fig. 1C, lower panel). The transfected TMEM55a was observed in the control cells but almost completely disappeared in TMEM55a-knockdown cells. Interestingly, the expression of FLAG–TMEM55a was increased in shTMEM55b cells, suggesting that FLAG–TMEM55a compensated for the deficit in TMEM55b. Hence, it is possible that the endogenous expression of TMEM55a may be also increased in shTMEM55b cells.

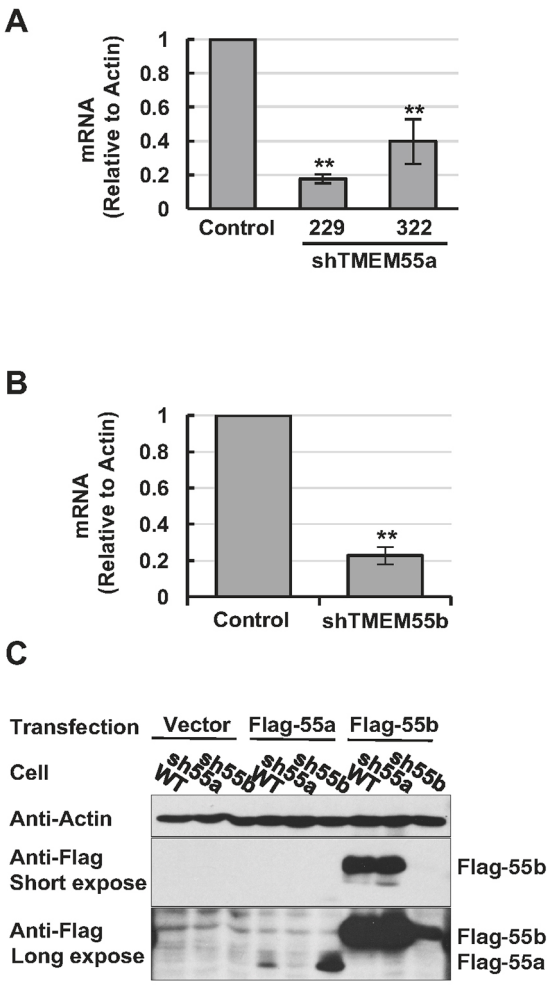

Fig. 1. Knockdown of TMEM55a and TMEM55b by shRNA in RAW264.7 macrophages. (A) Two lines of RAW264.7 cell lines deficient in TMEM55a (229 and 322) were generated by using the target sequences shown in Table S1. Quantitative RT-PCR was performed for TMEM55a mRNA, and results from three separate samples are shown as the means±s.e.m. (B) The relative amount of TMEM55b mRNA was calculated for a RAW264.7 cell line deficient in TMEM55b as in A. (C) Flag–TMEM55a or –TMEM55b was transfected to control cells (Raw264.7 with control pH1 plasmid, WT), shTMEM55a-229 (sh55a) or shTMEM55b (shTM55b) cells and incubated for 4 h. The cells were subjected to western blotting analysis with anti-actin (upper panel) or anti-FLAG antibody (middle and lower panels). The lower panel shows a long exposure of the middle panel. $^{**}P<0.01$.

The phagocytosis of large particles is increased in TMEM55a-deficient cells

The uptake of both IgG-RBCs (Fig. 2B) and non-opsonized zymosan particles (Fig. 2C) was elevated in these TMEM55a-deficient cells, whereas the binding of IgG-RBCs to these cells was comparable to that in wild-type (WT) cells (Fig. 2A), indicating that the amount of the surface Fcγ receptor was not increased in the knockdown cells. Cells defective in TMEM55b, another PtdIns(4,5)P_2 4-phosphatase, engulfed IgG-RBCs comparably to control cells (Fig. 2D). Thus, it is suggested that TMEM55a, but not TMEM55b negatively regulates phagocytosis. To further confirm the involvement of TMEM55a in phagocytosis, shTMEM55a cells were transfected with shRNA-resistant FLAG–TMEM55a. As shown in Fig. 2E,F, transfection of WT TMEM55a, but not its phosphatase dead mutant downregulated phagocytosis of IgG-RBCs both in control cells and shTMEM55a cells.

The phagocytosis of *E. coli* is unchanged in TMEM55a-deficient cells

In contrast to the engulfment of the large targets, phagocytosis of a smaller target, *E. coli*, was not affected by the TMEM55a depletion (Fig. 2G). It has been reported that class I PI3K-mediated inactivation of Rho family GTPases is essential to complete the phagocytosis of large particles whereas it is dispensable for the phagocytosis of smaller targets (Araki et al., 1996; Cox et al., 1999; Schlam et al., 2015). In fact, as seen in Fig. 2H, the class I PI3K inhibitor wortmannin severely inhibited IgG-RBC phagocytosis but did not affect the uptake of IgG-opsonized *E. coli* (IgG-*E. coli*) (Fig. 2I). Thus, it is likely that the upregulation of the phagocytosis in the knockdown cells may be explained by an increase of phagosomal PtdIns(3,4,5)P_3.

TMEM55a is involved in phagosomal PtdIns metabolism

We next investigated the phagosomal accumulation of PtdIns derivatives in TMEM55a-knockdown cells through live-cell imaging. For this purpose, EGFP-fused forms of MyoX(PH) and PLCδ(2×PH) were used as probes for PtdIns(3,4,5)P_3 and PtdIns(4,5)P_2, respectively. As presented in Fig. 3A, the control and

Journal of Cell Science (2018) 131, jcs213272. doi:10.1242/jcs.213272

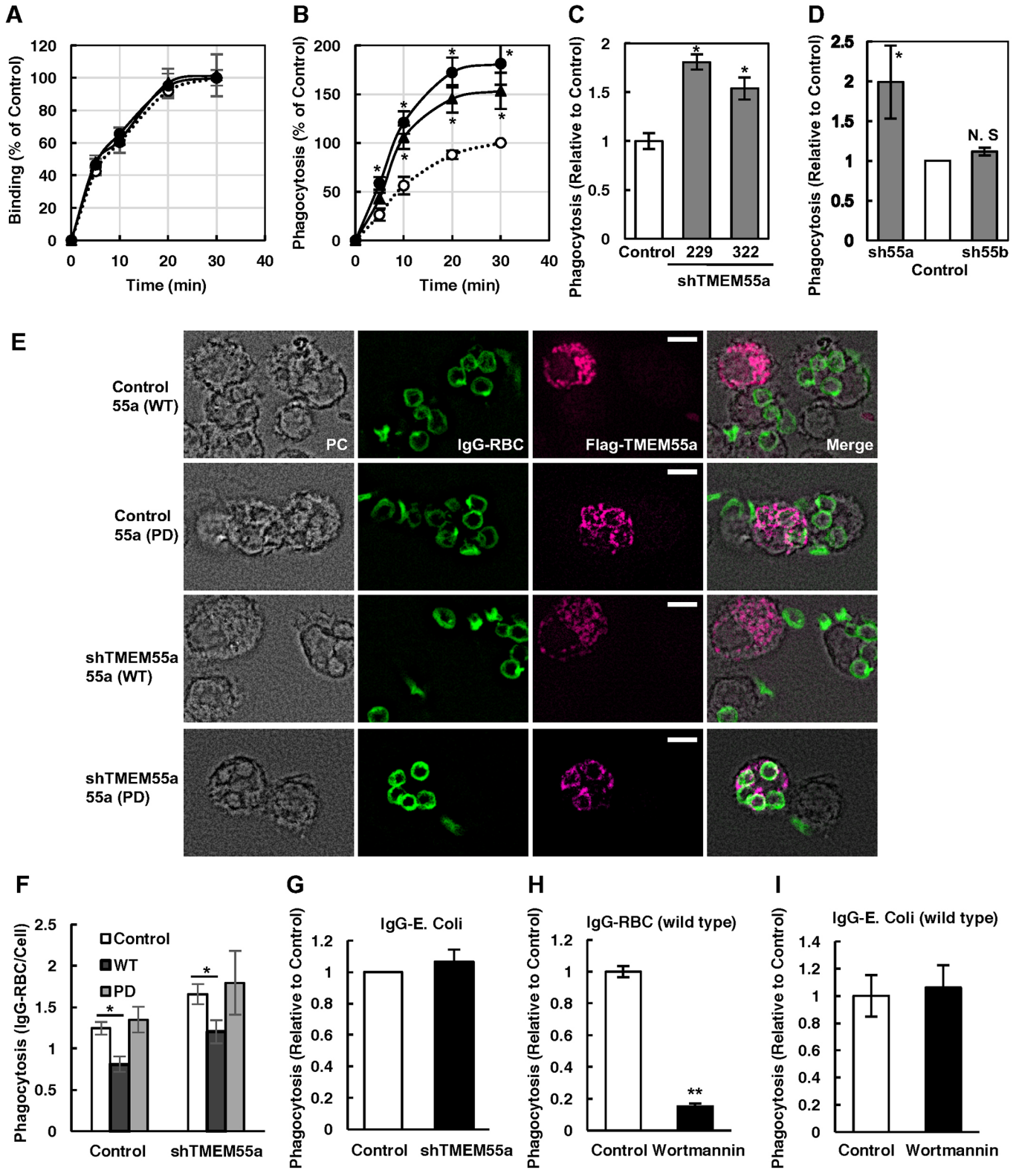

Fig. 2. See next page for legend.

the knockdown cells were transfected with EGFP–MyoX(PH). After the addition of IgG-RBCs, the fluorescence around the engulfed RBCs was monitored. In control cells, PtdIns(3,4,5)P_3 accumulated rapidly on the forming phagocytic cup but disappeared ~5 min after the onset of phagocytosis (Fig. 3A,B), as previously reported (Segawa et al., 2014). In TMEM55a-deficient cells, however, the phagosomal level of PtdIns(3,4,5)P_3 was higher than that in control cells and was maintained for far longer (Fig. 3A,B). Since it has not yet been demonstrated that endogenous TMEM55a dephosphorylates PtdIns(4,5)P_2 to PtdIns(5)P, we next examined

Fig. 2. Enhanced phagocytosis of large particles in TMEM55a knockdown cells. (A,B) Control (open circles) or TMEM55a-deficient cells (closed circle, 229 and closed triangle, 322) were incubated for the indicated times with ^{51}Cr-labeled IgG-RBCs. The number of IgG-RBCs on the outer surface of the cells (binding, A) and within the cells (phagocytosis, B) were determined as described in the Materials and Methods section. The values of control cells after a 30-min incubation are expressed as 100%. (C) Control or TMEM55a-knockdown cells were incubated with TexRed–zymosan for 15 min, and phagocytosis was determined as described in the Materials and Methods section. (D,H) Phagocytosis of IgG-RBCs in control, TMEM55a- or TMEM55b-knockdown cells was determined by performing microscopy analysis as described in the Materials and Methods section. (E,F) Control or shTMEM55a cells were transfected with shRNA-resistant FLAG-TMEM55a [WT or phosphatase dead (PD)], cultured for 4 h and incubated with IgG-RBCs. Phagocytosis by FLAG-TMEM55a expressing cells and non-expressing cells as shown in E was quantified from the images (F). PC, phase-contrast images. (G,I) Phagocytosis of IgG-opsonized *E. coli* was determined as described in the Materials and Methods section for WT and shTMEM55a cells. (H,I) WT Raw264.7 cells were treated with 30 nM wortmannin for 15 min at 37°C before addition of target particles. For all results, at least three independent experiments were performed. In C–I, the number of fluorescent particles was counted in merged images (each experiment used fluorescence images from at least 100 macrophages from three randomly selected fields) and the number of particles within the cells was calculated. In C,D,G,H,I, results are expressed as relative to the control cells. The results from three separate experiments are shown as the means±s.e.m. *P<0.05; N.S., not significant. Scale bars: 5 µm.

whether the phagosomal level of PtdIns(4,5)P_2 is altered in TMEM55a-knockdown cells (Fig. 3C,D). At the beginning of phagocytic cup formation, PtdIns(4)P on the plasma membrane is phosphorylated to PtdIns(4,5)P_2 on the cup (Coppolino et al., 2002). In control cells, PLCδ(PH) fluorescence on the phagosome peaked at 2 min and disappeared by ∼5 min after target incorporation (Fig. 3C). In cells lacking TMEM55a, the mean fluorescence on the phagocytic cup was higher than that on control cells. Additionally, the fluorescence surrounding phagosomes was prolonged after the completion of the incorporation in these cells (Fig. 3C). Expression of other lipid kinases and phosphatases that are involved in PtdIns(3,4,5)P_3 and PtdIns(4,5)P_2 production (PIP5K-I, class I PI3Ks and PTEN) was unchanged in shTMEM55a cells (Fig. S1). The total amount of PtdInsP_2 and PtdInsP at the steady state as determined by liquid chromatography mass spectrometry (LC/MS) system was almost comparable between the control cells and shTMEM55a cells (Fig. S2).

To further confirm TMEM55a as a phosphatase responsible for the dephosphorylation of PtdIns(4,5)P_2 to PtdIns(5)P on the phagosomes, we next tried to detect PtdIns(5)P. To date, visualization of PtdIns(5)P remains difficult but plant homodomain (PHD) finger of inhibitor of growth protein-2 (ING2) has been used as a bioprobe (Gozani et al., 2003). However, this probe sequesters PtIns(5)P, which limits the availability of the PtdIns and causes unfavorable effects on cytoskeleton organization (Viaud et al., 2014). To solve this problem, we tried a new overlay strategy: recombinant protein composed of 3×His-3×PHD was used to visualize PtdIns(5)P. A low-temperature expression system using chaperone plasmid and pCold™ vector enable creation of the recombinant protein. The construct was overlaid on the fixed cells and visualized with anti-His antibody and fluorescent secondary antibody. 3×PHD puncta surrounding zymosan particles were observed in the control cells (Fig. 4A, upper panels). It has been reported that the levels of PtdIns(5)P are profoundly decreased upon a hypo-osmotic stimulus (Sbrissa et al., 2002). To confirm 3×PHD puncta as PtdIns(5)P-containing endosomes, Raw264.7 cells were exposed to a hypo-osmotic medium after the engulfment. Surprisingly, 3×PHD was almost completely disappeared in these cells (Fig. 4A, lower panels). The validity of this probe was further supported by imaging of hydrogen peroxide-exposed cells, which have an increased PtdIns(5)P level (Jones et al., 2013), showing enormous accumulation of PtdIns(5)P in nuclei, as revealed by 3×PHD staining (Fig. 4B). Since the fluorescent intensity around zymosan was not bright enough to identify PtdIns(5)P-positive or -negative phagosomes in some cases, the profiling image of the phagosome was employed for the estimation (Fig. 4C). The phagosomes whose edges are brighter than the immediate outer areas were taken to be PtdIns(5)P-positive phagosomes (Fig. 4C). The quantitative analysis revealed that TMEM55a-deficient cells contained the less PtdIns(5)P on their phagosomes (Fig. 4D,E). When PtdIns(5)P was exogenously added to these cells, phagosomal PtdIns(5)P appeared to be increased (Fig. 4D). Hence, these results suggest that TMEM55a generates PtdIns(5)P on phagosomes.

Fcγ receptor-mediated Akt activation is enhanced in TMEM55a-knockdown cells

To further estimate PtdIns(3,4,5)P_3 production, WT and TMEM55a-deficient cells were stimulated with aggregated IgG, and phosphorylation of Akt family proteins was determined by western blotting. As shown in Fig. 5, the phosphorylation of Akt was activated in the knockdown cells. The phosphorylation of the p38 MAPK family proteins appeared to be slightly but not significantly activated. The enhanced phosphorylation of Akt in TMEM55a-deficient cells could be explained by the accumulation of PtdIns(4,5)P_2, which is immediately phosphorylated to PtdIns(3,4,5)P_3 by class I PI3K in the presence of Fcγ receptor ligation, because the expression of the PtdIns(3,4,5)P_3 phosphatase PTEN and that of class I PI3Ks was comparable in control and shTMEM55a cells (Fig. S1).

F-actin assembly on phagocytic cups is increased in TMEM55a-deficient cells

Upon IgG-RBC uptake, PtdIns(4,5)P_2 on the phagocytic cup promotes F-actin polymerization (Botelho et al., 2000; Szymańska et al., 2008), which is followed by its immediate disassembly induced by PtdIns(4,5)P_2 disappearance for cup closure (Araki et al., 1996; Schlam et al., 2015). To monitor the F-actin organization, cells were transfected with EGFP–Lifeact (Riedl et al., 2008) and challenged with IgG-RBC. The F-actin accumulation on the phagocytic cup was increased in TMEM55a-knockdown cells (Fig. 6). Unexpectedly, the disassembly occurred earlier in the knockdown cells than in control cells (Fig. 6B). Although the reason why the F-actin disappeared more rapidly in TMEM55a-deficient cells remains to be clarified, it is possible that the increased production of PtdIns(3,4,5)P_3, as observed in Figs 3 and 5, activated RhoGAP proteins, and hence led to the inactivation of Rho family GTPases and termination of actin assembly (Schlam et al., 2015). The increased F-actin organization and its prompt disassembly in TMEM55a-deficient cells is advantageous for the phagocytosis of large particles.

Transfected TMEM55a and TMEM55b accumulate on phagosomes

As mentioned above, a defect in TMEM55a, but not TMEM55b enhanced phagocytosis (Fig. 2D). The discrepancy between these cells may be explained by the following hypotheses: (1) that the intracellular localization of TMEM55a and TMEM55b is different, and only TMEM55a is involved in phagocytosis; (2) that the negative regulation of phagocytosis by TMEM55a is not dependent on its phosphatase activity but can be attributed to structures that are specific to TMEM55a; or (3) that the intrinsic activity of TMEM55a

Journal of Cell Science (2018) 131, jcs213272. doi:10.1242/jcs.213272

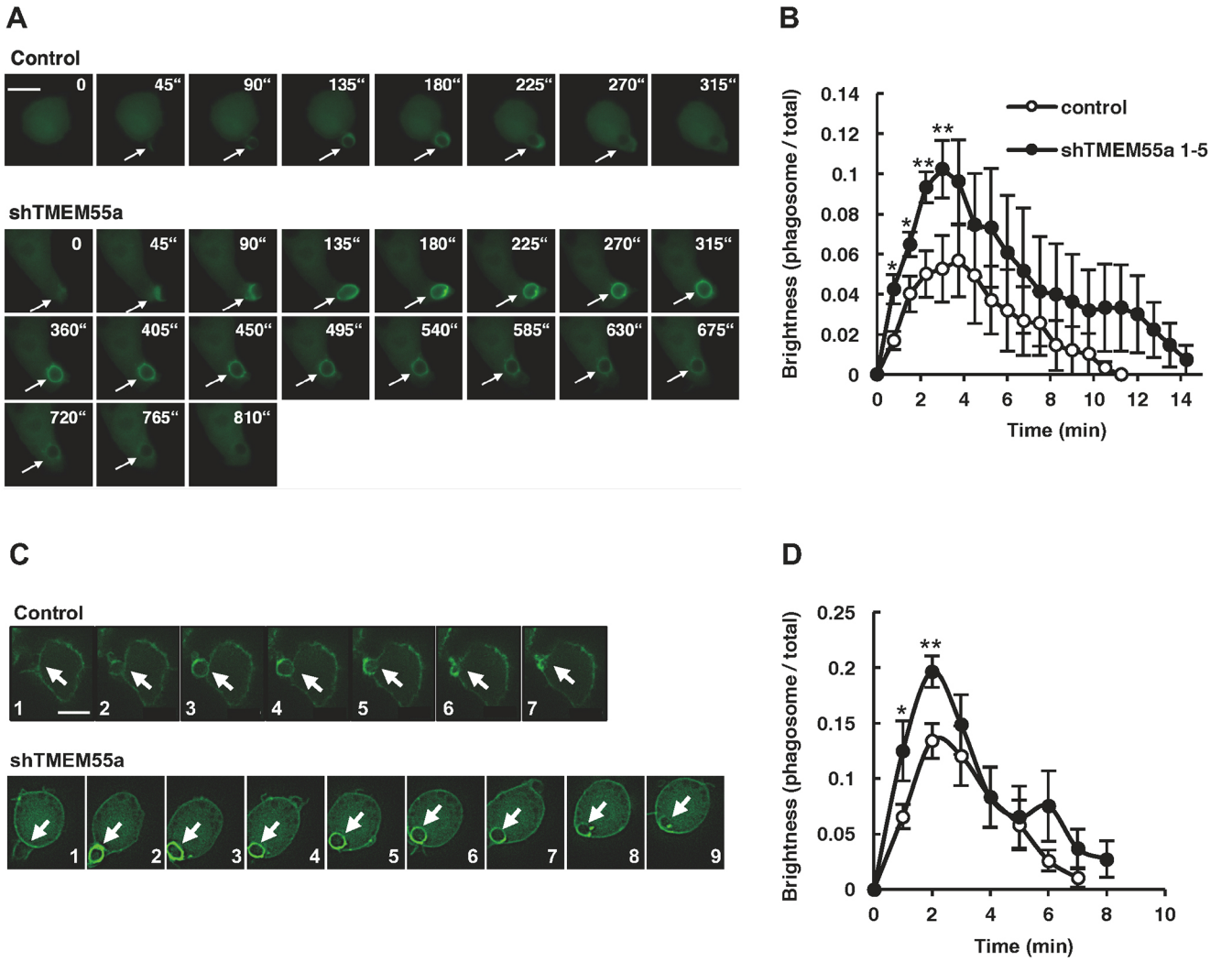

Fig. 3. Phagosomal levels of PtdIns(3,4,5)P_3 and PtdIns(4,5)P_2. Control or TMEM55a-deficient cells were transfected with EGFP–Myo X(PH) (A,B) or EGFP–PLCδ(2×PH) (C,D), cultured for 20 h and then challenged with IgG-RBCs. (A,C) Live-cell imaging. Fluorescent images were obtained every 45 s (A) or every 1 min (C). Arrows highlight phagocytic cups. (B,D) The phagosome-associated fluorescence intensity and total cellular fluorescence was quantified as described in the Materials and Methods section. The ratio of phagosome-associated fluorescence to total cellular fluorescence was calculated. The combined results from three separate experiments (each experiment analyzed three phagocytic cups) are shown as the means±s.e.m. *P<0.05, **P<0.01. Scale bars: 10 µm.

is superior to that of TMEM55b and compensates for the function of TMEM55b. To clarify which of these hypotheses was responsible for the observed results, we visualized the localization of fluorescently tagged TMEM55a and TMEM55b (Fig. 7). WT Raw264.7 cells were transfected with mCherry–TMEM55a or mCherry–TMEM55b along with EGFP–EEA1(fyve) which binds to PtdIns(3)P, and were fixed with paraformaldehyde without stimulation (Fig. 7A). The cells were then stained with anti-Lamp1 antibody and Alexa-Fluor-647-conjugated secondary antibody. Both TMEM55a and TMEM55b colocalized with Lamp1 but not with PtdIns(3)P (Fig. 7A, panels 1–5 and 11–15) suggesting that both phosphatases localized to late endosomes but not to early endosomes in the resting state. The cells were then transfected with mCherry–TMEM55s along with EGFP–PLCδ(PH) and immunostained with anti-Lamp1 antibody. In the steady state, TMEM55a partially co-existed with PtdIns(4,5)P_2 (Fig. 7A, panels 6–10, left-hand cell). The cells whose plasma membrane contained little TMEM55a showed more bright PLCδ(PH) fluorescence (panels 6–9, right-hand cell), suggesting the accumulation of PtdIns(4,5)P_2. This may be explained by dephosphorylation of PtdIns(4,5)P_2 by TMEM55a. In this context, it is likely that TMEM55b could not dephosphorylate PtdIns(4,5)P_2 because TMEM55b obviously colocalized with PLCδ(PH) on the plasma membrane (Fig. 7A, 16–20). Further quantitative analysis is needed for a conclusive answer to this issue, because the transfection efficiency was different from cell to cell. However, TMEM55a more or less localized to the plasma membrane and possibly dephosphorylated PtdIns(4,5)P_2 in the steady state.

The localization of TMEM55s during phagocytosis was next examined. WT Raw264.7 cells were transfected with the various Rab GTPases tagged with EGFP along with mCherry–TMEM55a or mCherry–TMEM55b, supplemented with IgG-RBC and fixed with paraformaldehyde. TMEM55a colocalized with Rab7a, which exist on the late phagosome and phagolysosome and play an indispensable role in the fusion of phagosomes and lysosomes (Fairn and Grinstein, 2012; Vieira et al., 2003) (Fig. 7B). TMEM55a also colocalized with early endosome marker Rab5b (Horiuchi et al., 1997) on phagosome membrane, although this occurred to a lesser extent (Fig. 7B). Rab20, which is another Rab family member that is recruited to the early endosome and has been

Journal of Cell Science (2018) 131, jcs213272. doi:10.1242/jcs.213272

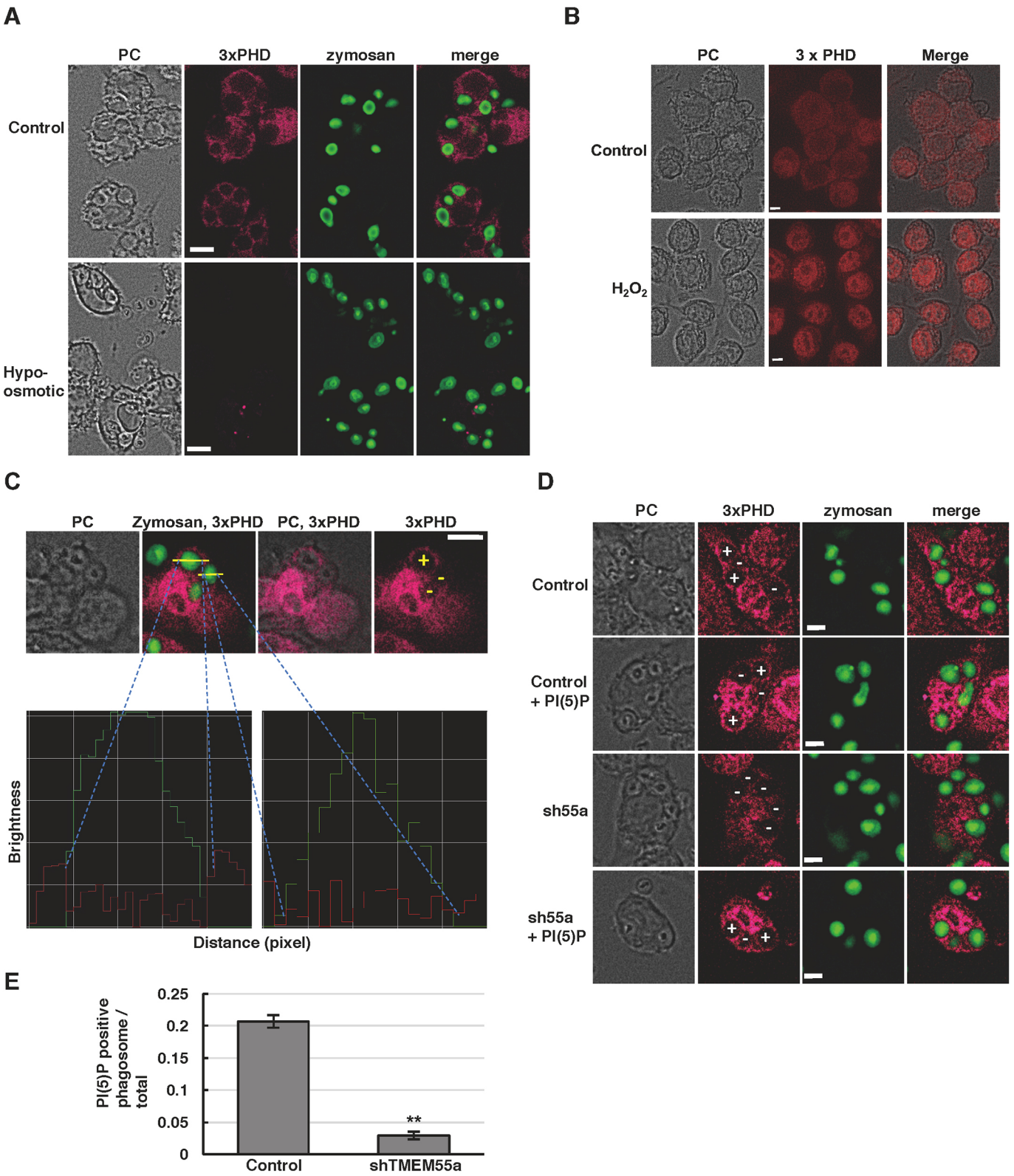

Fig. 4. Phagosomal levels of PtdIns(5)P. (A) After phagocytosis of FITC–zymosan, WT cells were exposed to normal (control) or 1:5 diluted medium (hypo-osmotic) for 5 min. The cells were fixed and PtdIns(5)P was visualized as described in the Materials and Methods section. (B) The cells were pre-treated with H_2O_2 for 40 min and stained with 3×His-3×PHD (3×PHD). (C) For the determination of PtdIns(5)P-positive and -negative phagosomes, a line was drawn across the image of the phagosome, and the brightness was determined along this line. (D,E) After the phagocytosis, control or TMEM55a-deficient cells were fixed and PtdIns(5)P was visualized. (E) The proportion of PtdIns(5)P-positive phagosomes of the total phagosomes was calculated. Control cells contained 60–142 zymosan particles, among which 13–28 phagosomes were PtdIns(5)P-positive. shTMEM55a cells contained 128–141 zymosans and 3–5 PtdIns(5)P-positive phagosomes. The combined results from three separate experiments are shown as the means±s.e.m. $^{**}P<0.01$. PC, phase-contrast images. In C,D,+in the 3×PHD image indicates PtdIns(5)P-positive phagosomes; – indicates PtdIns(5)P-negative phagosomes. Scale bars: 5 µm.

Journal of Cell Science (2018) 131, jcs213272. doi:10.1242/jcs.213272

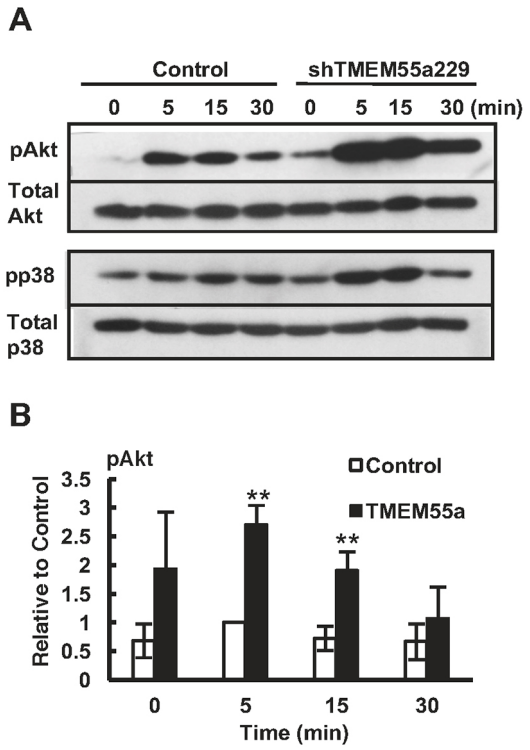

Fig. 5. Increased Fcγ receptor-mediated Akt phosphorylation in TMEM55a-knockdown cells. Control or TMEM55a-deficient cells were stimulated with 30 µg/ml aggregated IgG for the indicated times. (A) Total cell lysates were analyzed by western blotting using specific antibodies. (B) Phosphorylated Akt (pAkt) blots from A were analyzed using ImageJ and the level of pAkt was normalized to the total Akt band density. Results are expressed relative to the control value of 15 min-stimulated WT cells. The combined results from three separate experiments are shown as the mean±s.e.m. ***P*<0.01.

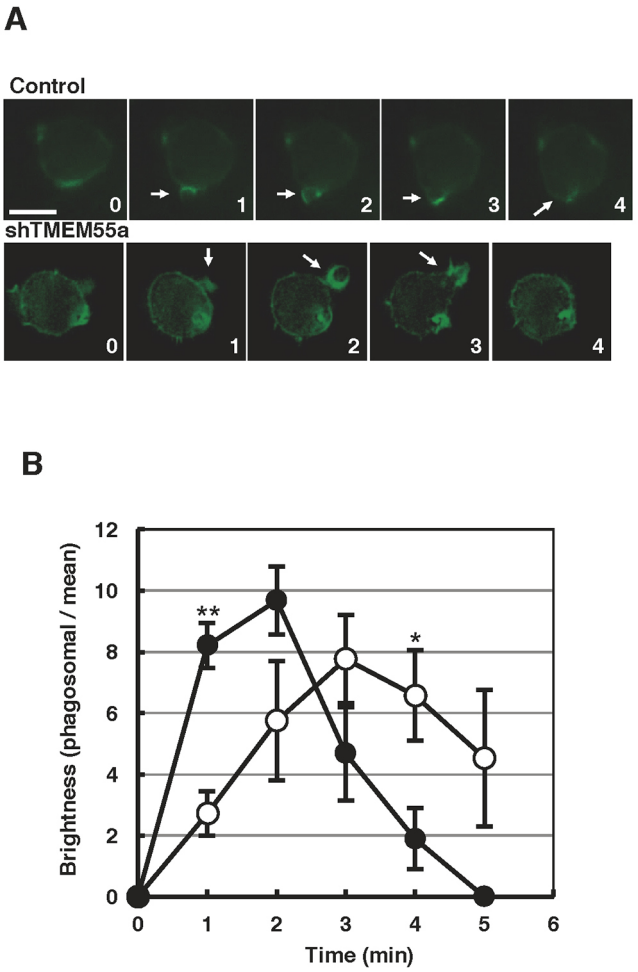

Fig. 6. Phagosomal levels of F-actin. Control or TMEM55a-deficient cells were transfected with EGFP–Lifeact, cultured for 20 h and then challenged with IgG-RBCs. (A) Live-cell imaging. Arrows highlight phagocytic cups. (B) The intensity of the phagosome-associated fluorescence and mean cellular fluorescence were quantified as described in the Materials and Methods section. Control (open symbol) and shTMEM55a (closed symbol). The ratio of phagosome-associated fluorescence to the mean cellular fluorescence was calculated. The combined results from three separate experiments (each experiment contains three phagocytic cups) are shown as the means±s.e.m. **P*<0.05. Scale bar: 10 µm.

reported to be responsible for regulating phagosome acidification (Egami and Araki, 2012; Segawa et al., 2014), partly colocalized with TMEM55a (Fig. 7B). Rab11a is recruited to recycling endosomes during phagocytosis (Cox et al., 2000) and colocalized with TMEM55a (Fig. 7B). TMEM55b showed similar localization to that of TMEM55a, in that it localized substantially with the late endosome marker Rab7 and partially with the other Rab family members (Fig. 7C).

Since TMEM55s localized to plasma membrane in the quiescent state (Fig. 7A), we next tested whether the phosphatases translocated to the phagocytic cup, where its substrate PtdIns(4,5)P_2 accumulated (Fig. 7D). Thus, we transfected TMEM55 proteins along with PLCδ(PH) to confirm the colocalization of the phosphatases and PtdIns(4,5)P_2 on the cup. As shown in Fig. 7D, TMEM55b obviously colocalized with PLCδ(PH) on plasma membrane and phagocytic cup, while TMEM55a was partly observed at the inner leaflet of plasma membrane. Additionally, TMEM55a only slightly colocalized with PLCδ(PH) on the phagocytic cup. We speculate that the enzymatic activity of TMEM55a is superior to TMEM55b and TMEM55a dephosphorylates PtdIns(4,5)P_2 on the plasma membrane and phagocytic cup. This might be the reason why we detect less colocalization of TMEM55a with PLCδ(PH) than we do for TMEM55b.

Another reason why we assumed TMEM55a to be the superior enzyme was that the overexpression of TMEM55a but not TMEM55b was lethal. Similar lethality was observed when IpgD was transfected into the cells. The expression of these PtdIns(4,5)P_2 phosphatases peaked at 4–5 h after the transfection and then declined by the time of cell death. In contrast, cells transfected with TMEM55b proliferate normally and the protein expression was excellent (Fig. 1C).

Overexpression of PtdIns(4,5)P_2 4-phosphatases inhibits, but PtdIns(5)P 4-kinase enhances, phagocytosis

To determine whether the negative regulation of phagocytosis by TMEM55a is dependent on its phosphatase activity, we next transfected IpgD, a PtdIns(4,5)P_2 phosphatase from *Sigella flexineri*, into Raw264.7 cells. The EGFP-tagged phosphatase was transfected to Raw264.7 cells, and the number of IgG-RBCs incorporated into the fluorescent cells was counted under a microscope (Fig. 8A). As shown in Fig. 8B, phagocytosis decreased in cells expressing IpgD. The expression of the phosphatase-dead mutants of IpgD did not affect the engulfment (Fig. 8B). Interestingly, the overexpression of PIP4K2a, which

Journal of Cell Science (2018) 131, jcs213272. doi:10.1242/jcs.213272

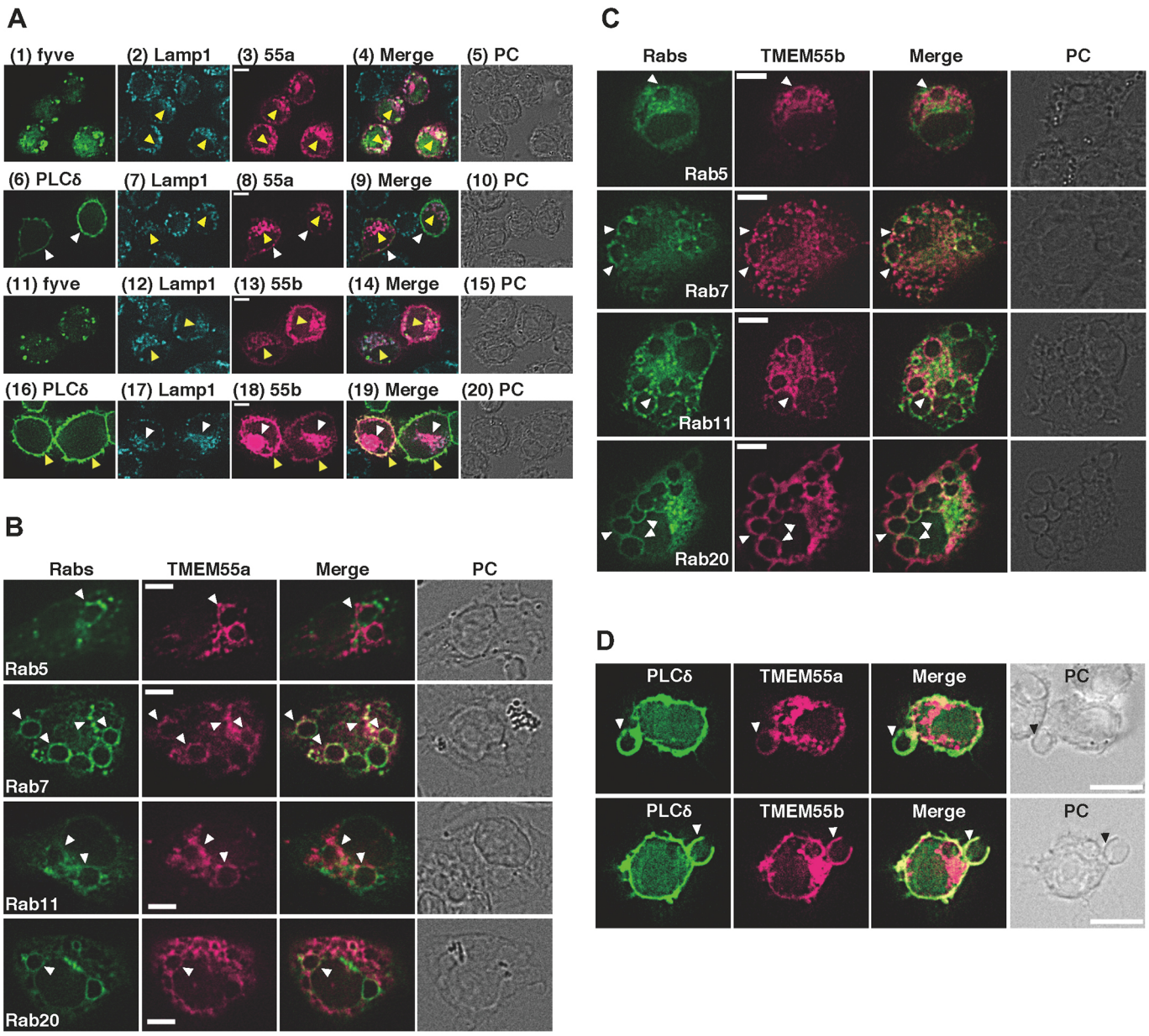

Fig. 7. Localization of TMEM55a and TMEM55b transfected into WT Raw264.7 cells. mCherry–TMEM55a (A,B,D) or mCherry–TMEM55b (A,C,D) was transfected into WT Raw264.7 cells along with EGFP-tagged Rab GTPases (B,C), EGFP–PLCδ(2×PH) (A,D) or EGFP–EEA1(3×fyve)] (A). Cells were then cultured for 5 h and then challenged with IgG-RBCs. Cells were fixed and immunostained with anti-Lamp1 antibody (A). To obtain improved optical resolution along the *z*-axis, *z*-stacks were captured at 1-µm steps over a *z*-axis distance of 5 µm, and the clearest planes are shown. In A, yellow arrowheads indicate the colocalization of TMEM55s with Lamp1, and white arrowheads indicate that of TMEM55a with PLCδ(2×PH). In B–D, arrowheads indicate the colocalization. PC, phase-contrast images. Scale bars: 5 µm (A–C), 10 µm (D).

phosphorylates PtdIns(5)P to PtdIns(4,5)P_2, increased phagocytosis (Fig. 8D). It is noteworthy that the transfected EGFP–PIP4K2a localized to phagosomes (Fig. 8C). These data strongly suggest that PtdIns(4,5)P_2 4-phosphatase inhibits but PtdIns(5)P 4-kinase enhances phagocytic activity. We next tested whether the product of PtdIns(4,5)P_2 4-phosphatase, PtdIns(5)P, inhibited phagocytosis. The cells were exogenously supplemented with C16-PtdIns(5)P along with carrier protein before undergoing a phagocytosis assay. Unexpectedly, the PtdIns(5)P-treatment did not inhibit phagocytosis either in WT or TMEM55a-deficient cells (Fig. 8E). It is speculated that PtdIns(4,5)P_2 accumulation rather than PtdIns(5)P deficiency may be responsible for the up-regulation of phagocytosis due to TMEM55a knockdown.

DISCUSSION

In this study, we discovered a new role for TMEM55a in phagocytosis. The following is our present perspective. TMEM55a localizes mainly to late endosomes and partially to the plasma membrane in a steady state (Fig. 7A). Upon the approach of target particles, the plasma membrane extends to form phagocytic cups containing TMEM55a (Fig. 7C). PtdIns(4)P on the phagocytic cup is phosphorylated to PtdIns(4,5)P_2, which accelerates F-actin assembly. TMEM55a then dephosphorylates PtdIns(4,5)P_2 to limit actin polymerization (Fig. 6), which ultimately downregulates phagocytosis (Fig. 2). In addition, since the assembly–disassembly cycle of F-actin is required for large particle ingestion, it is also likely that a decrease in PtdIns(4,5)P_2 results in decreased

Journal of Cell Science (2018) 131, jcs213272. doi:10.1242/jcs.213272

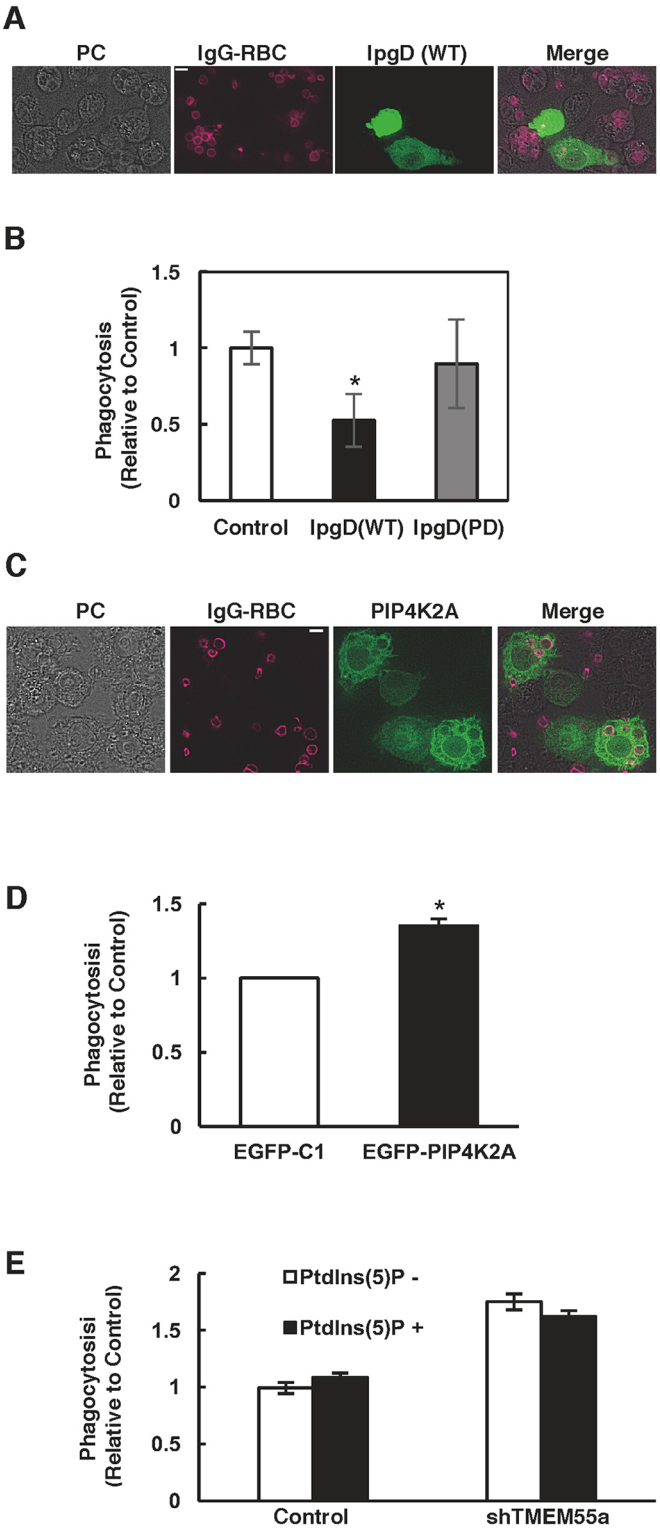

Fig. 8. Overexpression of the PtdIns(4,5)P_2 4-phosphatases inhibits whereas PtdIns(5)P 4-kinase enhances phagocytosis. WT Raw264.7 cells were transfected with EGFP-tagged IpgD (A,B), its phosphatase-dead mutant (PD) (B) or EGFP-tagged PIP4K2a (C,D), cultured for 5 h, and incubated with IgG-RBCs. Phagocytosis by EGFP-expressing cells and non-expressing cells as shown in A,C was quantified from the images. (E) WT cells were treated with C16-PtdIns(5)P along with the carrier protein as described in the Materials and Methods section. Phagocytic activity against IgG-RBCs was determined quantified from the images. In B,D and E, results from three separate experiments (each experiment used fluorescence images of at least 100 macrophages from three randomly selected fields) are shown as the means±s.e.m. PC, phase-contrast images. *P<0.05. Scale bars: 5 µm.

PtdIns(3,4,5)P_3 production (Fig. 3), which in turn perturbs the RhoGAP-coordinated disassembly of F-actin and dampens phagocytosis in a target size-dependent manner (Fig. 2). This speculation is based on the experiments using TMEM55a-deficient cells. These cells exhibited enhanced phagocytic activity, accompanied by increased accumulation of PtdIns(4,5)P_2, PtdIns(3,4,5)P_3 and F-actin on the phagocytic cup. The finding that the overexpression of PIP4K2a, which catalyzes the reverse reaction from that of TMEM55a, also increased phagocytosis supports the hypothesis (Fig. 8C,D). Additional support is provided by the results seen upon ectopic expression of IpgD, a PtdIns(4,5)P_2 4-phosphatase from bacteria, which inhibited the phagocytosis in a manner dependent on its enzymatic activity (Fig. 8A,B).

It is generally accepted that PtdIns(4,5)P_2 is responsible for the assembly and remodeling of F-actin during the formation of nascent phagosomes (Tuosto et al., 2015). The amount of PtdIns(4,5)P_2 on a phagocytic cup is regulated by various lipid kinases and phosphatases. Among these, PtdIns(4)P 5-kinases have been previously implicated in phagocytosis. In Raw264.7 macrophages, we detected small quantities of PtdIns(4)P 5-kinase β, as reported previously (Mao et al., 2009). Instead, the α and γ subtypes are more likely involved in phagocytosis. Bone marrow-derived macrophages from PtdIns(4)P 5-kinase γ-knockout mice have a highly polymerized actin cytoskeleton and are defective in IgG-RBC binding to the Fcγ receptor (Mao et al., 2009). In contrast, PtdIns(4)P 5-kinase α knockout has no effect on binding, but instead inhibits phagocytosis by decreasing Wiskott–Aldrich syndrome protein (WASP) and Arp2/3 activation, which, in turn, impairs *de novo* actin polymerization at the phagocytic cup (Mao et al., 2009). Hence, we speculate that PtdIns(4,5)P_2 produced by PtdIns(4)P 5-kinase is dephosphorylated by TMEM55a, which results in diminished F-actin assembly for large phagocytic cup formation.

The quiescent level of PIP_2, which is mostly PtdIns(4,5)P_2, shown in Fig. S2 was slightly but significantly lower in shTMEM55a cells than that in control cells. Since TMEM55a dephosphorylates PtdIns(4,5)P_2 to PtdIns(5)P, the reason for this is so far not known. However, it has been reported that a decrease in PtdIns(5)P dampens PtdIns(4,5)P_2 production (Sbrissa et al., 2002). Since most of PtdIns(4,5)P_2 is generated by PIP5K-mediated phosphorylation of PtdIns(4)P, it is intriguing to speculate that the PIP5K activity is regulated by PtdIns(5)P indirectly. A comprehensive analysis of protein–protein interaction recently revealed that PIP4K2a, PIP4K2b and PIP4K2c, which generate PtdIns(4,5)P_2 from PtdIns(5)P, associate with PIP5K (Huttlin et al., 2017). The decreased PIP_2 in the knockdown cells may be related to such an interaction.

TMEM55b is another PtdIns(4,5)P_2 4-phosphatase with similar localization to TMEM55a (Fig. 7B). However, a reduction in TMEM55b expression did not increase phagocytosis (Fig. 2D). It is likely that the intrinsic enzymatic activity of TMEM55a is more robust than that of TMEM55b and can compensate for a loss in TMEM55b function. This concept is supported by the finding that the expression of transfected TMEM55a was increased in shTMEM55b cells compared to that in WT cells (Fig. 1C).

TMEM55a and TMEM55b were originally reported to be involved in endosome maturation (Ungewickell et al., 2005).

Since both the phosphatases localize to phagosomes during phagocytosis (Fig. 7), it is reasonable that they also function in the maturation process. Further studies should investigate the function of TMEM55 proteins in phagosome acidification, the exchange of Rab GTPases, and Lamp1 or Lamp2 recruitment to phagosomes.

MATERIALS AND METHODS

Materials

The sources of materials were as follows: zymosan, TexRed–zymosan, fluorescein isothiocyanate (FITC)–zymosan, *E. coli*-opsonizing reagent (E-2870), and RPMI 1640 medium (Life Technologies Co., Carlsbad, CA); protein assay kit (Bio-Rad, Hercules, CA); sheep red blood cells (RBCs) (Cosmo Bio Co., Tokyo, Japan); Alexa Fluor 488-conjugated anti-rabbit IgG and anti-pAkt (1:1000, #9271; Cell Signaling, Danvers, MA); anti-SRBC (1:50, A-6840, InterCell Technologies, Jupiter, FL); anti-pp38 (1:2500, #612280; BD Transduction Laboratories, Franklin Lakes, NJ); anti-Flag M2 monoclonal antibody (1:1000, #F3165; Sigma Aldrich, Japan); anti-actin antibody (1:5000, #612656; BD Transduction Laboratories); anti-Lamp 1 antibody (1:500, #121601, BioLegend, San Diego, CA); $Na_2{}^{51}CrO_4$ (MP Biomedicals, Santa Ana, CA); Shuttle PIP™ and C16-PtdIns(5)P (Echelon Scientific, UT).

Cells

RAW264.7 cells (ATCC #2142765) lacking TMEM55a or TMEM55b were produced as follows (Kubo et al., 2005). Oligonucleotides targeting each molecule (Table S1) were cloned into a pH1 vector downstream of the H1 RNA promoter as previously described to express small interfering RNA (siRNA) hairpins. For each of the targeted sequences, a pair of oligonucleotides were synthesized (eurofins, Tokyo, Japan) with the following sequences: 5′-CCC$(X)_{19}$TTCAAGAGA$(Y)_{19}$TTTTTGGAAA-3′ and 5′-CTAGTTTCCAAAAA$(Y)_{19}$TCTCTTGAA$(X)_{19}$GGGTGCA-3′, where $(X)_{19}$ is the coding sequence and $(Y)_{19}$ is the complementary sequence. This oligonucleotide pair was annealed and ligated downstream of the H1 RNA promoter at the PstI and XbaI sites of the pH1 vector. Plasmids were transfected into RAW264.7 cells (5×10^6–10×10^6 cells) at 250 V/950 µF (Gene Pulser II; Bio-Rad). At 24 h after transfection, puromycin (3 µg/ml) was added to the cells, and the incubation was continued to select for resistant cells. To determine the gene silencing efficiency, total RNA was isolated with Sepasol (Nakarai Tesque, Kyoto, Japan), and the mRNA was quantified by reverse transcription PCR with the primer pairs shown in Table S2. Control cells were prepared as above with a pH1 vector containing a 400-bp stuffer sequence instead of the target sequence. For microscopic analysis, cells were seeded in tissue culture-coated glass bottom dishes (Greiner Bio-One, Frickenhausen, Germany) in RPMI 1640 medium containing 4.5 g/l glucose and 10% fetal calf serum (FCS) in a humidified 5% CO_2 atmosphere at 37°C. Immediately before starting the assay, media were aspirated and replenished with incubation buffer (complete RPMI 1640 medium without $NaHCO_3$, fortified with 20 mM HEPES-NaOH, pH 7.4). Activities were then determined by incubating the cells at 37°C under ambient conditions. Alternatively, cells were seeded in 24-well plates in normal RPMI 1640 medium to determine the level of Akt phosphorylation in response to aggregated IgG. The incubation was then undertaken as above in the incubation buffer.

Preparation of IgG-RBCs and measurement of phagocytosis using ^{51}Cr

Sheep red blood cells (RBCs) were labeled with ^{51}Cr as previously described (Ninomiya et al., 1994). IgG-RBCs were prepared by incubating labeled cells with rabbit anti-SRBC antibody at 37°C for 10 min in 5 mM veronal buffer (pH 7.5) supplemented with 0.1% gelatin, 75 mM NaCl, 0.15 mM $CaCl_2$, 0.5 mM $MgCl_2$ and 10 mM EDTA, followed by incubation on ice for 15 min. The IgG-RBCs were washed three times with 5 mM veronal buffer (pH 7.5) supplemented with 0.1% gelatin, 75 mM NaCl, 0.15 mM $CaCl_2$, and 0.5 mM $MgCl_2$ (GVB) and finally suspended in incubation buffer (detailed above). The binding and phagocytosis of IgG-RBCs were measured as previously reported (Niomiya et al., 1994). RAW264.7 cell monolayers (2×10^5 cells/well in a 24-well plate) were incubated with ^{51}Cr-labeled IgG-RBCs (2×10^7 cells) at 37°C for the indicated times. Monolayers were then washed three times with PBS to remove unbound IgG-RBCs and then briefly exposed to 0.1 ml of hypotonic PBS (diluted fivefold). The radioactivity released into the supernatant during the hypotonic shock was measured as a proxy for the amount of IgG-RBCs bound to the surface of the phagocytes. Monolayers were washed an additional three times with PBS and finally solubilized in 0.5% Triton X-100. Solution radioactivity was measured to determine the amount of engulfed IgG-RBCs.

Measurement of phagocytosis of IgG-RBCs by microscopy

As shown in Figs 2E and 8, cells were transfected with FLAG-tagged or EGFP-tagged constructs and seeded into tissue culture-coated glass bottom dishes 4–6 h before the phagocytosis assay. Cells were incubated with non-labeled IgG-RBCs prepared as above and kept on ice for 15 min, followed by an incubation at 37°C for 15 min. Cells were then washed three times with PBS, fixed with PBS containing 4% formaldehyde for 15 min at room temperature, permeabilized with TBS containing 0.1% saponin and 3% BSA for 60 min and finally subjected to immunostaining with Alexa Fluor 647-conjugated anti-rabbit IgG to assess the IgG-RBC engulfment. In Fig. 2E, FLAG tag was immunostained with anti-FLAG antibody (1:1000, Sigma #F3165) and Alexa Fluor 488-conjugated anti-mouse IgG (Cell Signaling) secondary antibody. The numbers of engulfed IgG-RBCs were determined by using a BZ-H2C analysis system (Keyence, Osaka, Japan).

Phagocytosis of zymosan

TexasRed- or FITC-labeled zymosan particles were mixed with an equal amount of unlabeled zymosan to expedite counting, and the mixture was sonicated for ∼1 min. RAW264.7 cells (10^5 cells/well in a glass bottom dish) were incubated at 37°C for the indicated durations with 2×10^6 zymosan particles. Phagocytosis was stopped by the addition of ice-cold PBS. Cells were then washed three times with PBS, fixed with 4% paraformaldehyde for 15 min at room temperature and finally rinsed with PBS. Fluorescence and phase-contrast images of at least 100 macrophages from three randomly selected fields were taken using confocal microscopy. The mean numbers of ingested zymosan particles were expressed as particles per RAW264.7 cell.

Phagocytosis of *E. coli*

mCherry was amplified by PCR using oligonucleotide primers, introducing BamHI and EcoRI sites at the 5′ and 3′ ends, respectively, with pmCherry-N1 (Clontech, Mountain View, CA) as a template. Amplification products were then cloned into the pGEX-4T-3 vector. The resulting recombinant plasmid was then used to transform BL-21 *E. coli*. Induction of mCherry was carried out as follows. A single colony was inoculated into 10 ml of Luria–Bertani (LB) medium and grown overnight at 37°C. Bacteria were expanded in 100 ml of LB medium and growth was allowed to continue at 37°C until the optical density at 600 nm (OD_{600}) reached 0.8. Protein expression was induced by the addition of isopropyl-β, d-thiogalactopyranoside at a final concentration of 0.5 mM and incubation was continued for an additional 4 h at 30°C. mCherry-expressing *E. coli* were then washed and fixed with 4% paraformaldehyde for 15 min at room temperature and stored at 4°C in the presence of NaN_3 until use. Labeled *E. coli* were opsonized with the opsonizing reagent in GVB, washed with the same buffer and sonicated for 3 min immediately before use. Raw264.7 cells in glass bottom dishes were incubated with labeled *E. coli* (1:50 ratio) at 0°C for 20 min, transferred to 37°C and further incubated for 20 min. The phagocytosis was stopped by washing three times with acidic medium (pH 5.5) to strip the binding *E. coli*. Cells were fixed in 4% paraformaldehyde for 15 min at room temperature and finally rinsed with PBS. Fluorescence images and phase-contrast images of at least 100 macrophages from three randomly selected fields were taken using confocal microscopy.

Delivery of PtdIns(5)P into Raw264.7 macrophages

C16-PtdIns(5)P was dissolved in $CHCl_3$:MeOH:H_2O (1:2:0.8), and aliquots were stored at −80°C. The solvent was dried with liquid nitrogen gas. The

dried PtdIns(5)P was mixed with the carrier at a 1:1 molar ratio, sonicated for 2 min and incubated 10 min at room temperature. The resulting phosphoinositide–carrier complex was then diluted in medium and added to cells (Vicinanza et al., 2015).

Plasmids

The tandem domain of myosin X, PH1(N)-PH2-PH1(C) (Cox et al., 2002; Lu et al., 2011), hereafter referred to as MyoX(PH), was isolated from mouse macrophages by RT-PCR with the following primer pair: 5′-AGATCTCC-CTATTTCCACAGTTTTC-3′ and 5′-GAATTCCTACTTGGATCTCTGC-AGCA-3′. This domain was then subcloned into pEGFP-C1 (Clontech) at the BglII and EcoRI sites. pEGFP-C1-IpgD (WT and phosphatase dead mutants), pEGFP-N1-PLCδ(PH), and TMEM55a, TMEM55b and PIP4K2a from mouse origin cloned into pcDNA3.1 were kindly provided by Dr Takehiko Sasaki (Akita University, Akita City, Japan). TMEM55a and TMEM55b were subcloned into pmcherry-C1 at the EcoRI and BamHI sites and the HindIII and BamHI sites, respectively. For the rescue experiments, silent mutations were introduced into the target sequence of TMEM55a constructs using primer pair shown in Table S3. PIP4K2a was subcloned into pEGFP-C1 at the KpnI and XbaI sites. The EGFP-tagged Rab5, Rab7, Rab11 and Rab20 constructs were kind gifts from Dr Mitsunori Fukuda (Tohoku University, Sendai, Japan) (Fukuda et al., 2008). EGFP-Lifeact was prepared as previously described (Riedl et al., 2008).

Transfection

Plasmids were transfected using the Neon™ transfection system (Invitrogen). Briefly, Raw264.7 cells were suspended in 25 µl of T buffer at 5×10^7 cells/ml and mixed with 2 µg of plasmid DNA. Cells were then subjected to electroporation using a single 20-ms pulse of 1800 V with a 10 µl tip two times. Electroporated cells were immediately transferred to culture-coated glass bottom dishes (~2 cm^2) in RPMI 1640 medium containing 20% FCS without antibiotics. At 5–24 h (the incubation length varied depending on the plasmid) after transfection, cells were subjected to microscopic analysis.

Monitoring PtdIns dynamics during the course of phagocytosis

Cells were incubated with IgG-RBCs and placed on a BIOREVO BZ9000 microscope (Keyence, Osaka, Japan) equipped with a CFI Plan Apo VC60×H oil immersion lens, and phagocytosis was allowed to proceed at 37°C (Segawa et al., 2017). Unless otherwise stated, the fluorescent images were collected every 1 min, and the intensity of the phagosome-associated fluorescence was analyzed by using a BZ-II analysis system (Keyence, Osaka, Japan).

PtdIns(5)P determination using 3×His-3×PHD

pEGFP-C1-3×PHD was kindly donated by Dr Bernard Payrastre (Université Paul Sabatier, Toulouse, France) (Gozani et al., 2003). 3×PHD was amplified by PCR using oligonucleotide primers with the sequences 5′-GGTACCCGGACTCAGATCTCGGCA-3′ and 5′-GGATCCCCGTCGA-CTCATCACTAC-3′. The amplification product was then cloned into pCold II vector (Takara) at the KpnI and BamHI sites. The resulting recombinant plasmid was used to transform BL-21 previously transformed with chaperone plasmid (pG-KJE8, Takara) and cultured overnight on LB plates fortified with chloramphenicol (50 µg/ml) and ampicillin (50 µg/ml). Induction of 3×His-3×PHD was carried out as follows. A single colony was inoculated into 10 ml of LB medium with chloramphenicol and ampicillin and grown overnight at 37°C. Bacteria were expanded in 100 ml of LB medium containing chloramphenicol, ampicillin, arabinose (0.5 mg/ml) and tetracycline (5 ng/ml). Growth was allowed to continue at 37°C until the OD_{600} reached 0.5–0.7, at which point the culture was transferred to 15°C for an additional 30 min. Protein expression was induced by the addition of isopropyl-β, D-thiogalactopyranoside at a final concentration of 0.5 mM and incubation was continued for a further 24 h at 15°C. The purification of 3×His-3×PHD was performed using TALON metal affinity resin (Clontech) according to the manufacturer's protocol. Briefly, the cells were collected by centrifugation (5000 ***g*** for 5 min), resuspended in 4 ml of lysis buffer (50 mM $NaH_2PO_4{\cdot}H_2O$, 300 mM NaCl, 10 mM imidazole, 0.5% Triton X-100 and 1 mM PMSF, pH 7.4) and sonicated for 3 min. After centrifugation (15,000 ***g*** for 30 min), the supernatant was mixed with a 2 ml bed of TALON resin pre-washed with lysis buffer, and then incubated at 4°C for 30 min with rotation. After three washes with lysis buffer, the bound proteins were eluted with lysis buffer supplemented with 160 mM imidazole. The eluate was then passed through a PD-10 column (GE Healthcare) to remove imidazole. The prepared protein was identified as single band by Coomassie Blue staining after SDS-PAGE. The purified protein was identified as a single band by Coomassie Blue staining after SDS-PAGE and by western blotting with anti-His antibody (Amersham Biosciences).

After phagocytosis of FITC-zymosan, cells were washed thrice with acidic medium (pH 5.5) to strip binding zymosan. Cells were fixed with 4% paraformaldehyde for 15 min at room temperature, rinsed with PBS and permeabilized with PBS containing 0.1% saponin and 3% BSA for 30 min. After incubation with 3×His-3×PHD described above at 4°C overnight, the cells were washed three times with 0.1% saponin in PBS, incubated with anti-His antibody (1:1000, #27-4710-01, GE Healthcare) for 4 h and finally stained with Alexa Fluor 647-labeled secondary antibody (1:1000 dilution) for 2 h at room temperature. Microscopic analysis was performed by using a Keyence BZ-9000 fluorescence microscope with CFI Plan Apo VC60×H lens (Keyence, Osaka, Japan). Fluorescence images of at least 100 macrophages from three randomly selected fields were counted to analyze the PtdIns(5)P-positive phagosomes.

Western blotting

Cells in the 24-well plates were incubated with 30 µg/ml aggregated mouse IgG, which was prepared by heating at 62°C for 30 min. Cells were then washed with PBS and lysed in 50 µl of lysis buffer containing 25 mM Tris-HCl pH 7.4, 0.5% Nonidet P-40, 150 mM NaCl, 1 mM sodium orthovanadate (Na_3VO_4), 1 mM EDTA, 20 mM sodium fluoride, 1 mM phenylmethylsulfonyl fluoride, protease inhibitor cocktail (Sigma-Aldrich) and 20 µM p-amidinophenylmethylsulfonyl fluoride. Cell lysates were centrifuged at 20,000 ***g*** for 10 min. Supernatants were collected, and the protein concentration was determined by using a Bio-Rad assay kit. Total cell lysates (100 µg protein) were mixed with 10 µl of 5× sample buffer (62.5 mM Tris-HCl pH 6.8, 1% SDS, 10% glycerol, 5% 2-mercaptoethanol, and 0.02% Bromophenol Blue) and heated at 100°C for 5 min. Proteins were separated by SDS-PAGE and transferred electrophoretically onto a polyvinylidene difluoride (PVDF) membrane (Millipore). This membrane was blocked with 5% skimmed milk and incubated with the appropriate antibodies. Antibody binding was detected by using a chemiluminescent substrate (Perkin-Elmer).

Quantitative RT-PCR

Total RNA prepared from the indicated cells was subjected to quantitative RT-PCR analysis. In brief, cDNA were amplified with FastStart Universal SYBER Green Master and primer sequences provided in Table S2 by ABI HT-7900. Data analysis was performed using the ΔΔCT methods as described in the Applied Biosystem protocol. A ΔCT value was determined for each sample using the CT value from input DNA. The CT value for β-actin was used to normalize RT-PCR loading. ΔΔCT values were then obtained by subtracting control ΔCT values (vector control) from sample ΔCT values from the knockdown cells. The ΔΔCT values were converted to fold difference compared with the control by raising 2 to the ΔΔCT power.

Statistical analysis

Two-tailed Student's *t*-tests were performed. All *P*-values were considered significant at $P<0.05$.

Acknowledgements

We thank Dr Takehiko Sasaki (Akita University) for pEGFP-C1-IpgD (wild type and phosphatase dead mutants), pEGFP-N1-PLCδ(PH), TMEM55a, TMEM55b and PIP4K2a, Dr Mitsunori Fukuda (Tohoku University) for EGFP-Rab5, Rab7, Rab11 and Rab20, and Dr Bernard Payrastre (Université Paul Sabatier) for EGFP-3×PHD.

Competing interests

The authors declare no competing or financial interests.

Author contributions

Conceptualization: K.H.; Methodology: H.N., K.H.; Validation: K.H.; Formal analysis: K.H.; Investigation: S.M., K.N., E.O., Y.T., Y.K., M.Y., H.N., K.H.; Resources: S.T., T.S., K.H.; Data curation: K.N., K.H.; Writing - original draft: K.H.; Writing - review & editing: K.H.; Visualization: K.H.; Supervision: K.H.; Project administration: K.H.; Funding acquisition: S.K.

Funding

S.K. was supported, in part, by Home for Innovative Researchers and Academic Knowledge Users (HIRAKU).

Supplementary information

Supplementary information available online at
http://jcs.biologists.org/lookup/doi/10.1242/jcs.213272.supplemental

References

Araki, N., Johnson, M. T. and Swanson, J. A. (1996). A role for phosphoinositide 3-kinase in the completion of macropinocytosis and phagocytosis by macrophages. *J. Cell Biol.* **135**, 1249-1260.

Boal, F., Mansour, R., Gayral, M., Saland, E., Chicanne, G., Xuereb, J.-M., Marcellin, M., Burlet-Schiltz, O., Sansonetti, P. J., Payrastre, B. et al. (2015). TOM1 is a PI5P effector involved in the regulation of endosomal maturation. *J. Cell Sci.* **128**, 815-827.

Botelho, R. J., Teruel, M., Dierckman, R., Anderson, R., Wells, A., York, J. D., Meyer, T. and Grinstein, S. (2000). Localized biphasic changes in phosphatidylinositol-4,5-bisphosphate at sites of phagocytosis. *J. Cell Biol.* **151**, 1353-1368.

Coppolino, M. G., Dierckman, R., Loijens, J., Collins, R. F., Pouladi, M., Jongstra-Bilen, J., Schreiber, A. D., Trimble, W. S., Anderson, R. and Grinstein, S. (2002). Inhibition of phosphatidylinositol-4-phosphate 5-kinase Ialpha impairs localized actin remodeling and suppresses phagocytosis. *J. Biol. Chem.* **277**, 43849-43857.

Cox, D., Tseng, C.-C., Bjekic, G. and Greenberg, S. (1999). A requirement for phosphatidylinositol 3-kinase in pseudopod extension. *J. Biol. Chem.* **274**, 1240-1247.

Cox, D., Lee, D. J., Dale, B. M., Calafat, J. and Greenberg, S. (2000). A Rab11-containing rapidly recycling compartment in macrophages that promotes phagocytosis. *Proc. Natl. Acad. Sci. USA* **97**, 680-685.

Cox, D., Berg, J. S., Cammer, M., Chinegwundoh, J. O., Dale, B. M., Cheney, R. E. and Greenberg, S. (2002). Myosin X is a downstream effector of PI(3)K during phagocytosis. *Nat. Cell Biol.* **4**, 469-477.

Egami, Y. and Araki, N. (2012). Rab20 regulates phagosome maturation in RAW264 macrophages during Fc gamma receptor-mediated phagocytosis. *PLoS ONE* **7**, e35663.

Fairn, G. D. and Grinstein, S. (2012). How nascent phagosomes mature to become phagolysosomes. *Trends Immunol.* **33**, 397-405.

Freeman, S. A. and Grinstein, S. (2014). Phagocytosis: receptors, signal integration, and the cytoskeleton. *Immunol. Rev.* **262**, 193-215.

Fukuda, M., Kanno, E., Ishibashi, K. and Itoh, T. (2008). Large scale screening for novel rab effectors reveals unexpected broad Rab binding specificity. *Mol. Cell. Proteomics* **7**, 1031-1042.

Gozani, O., Karuman, P., Jones, D. R., Ivanov, D., Cha, J., Lugovskoy, A. A., Baird, C. L., Zhu, H., Field, S. J., Lessnick, S. L. et al. (2003). The PHD finger of the chromatin-associated protein ING2 functions as a nuclear phosphoinositide receptor. *Cell* **114**, 99-111.

Horiuchi, H., Lippé, R., McBride, H. M., Rubino, M., Woodman, P., Stenmark, H., Rybin, V., Wilm, M., Ashman, K., Mann, M. et al. (1997). A novel Rab5 GDP/GTP exchange factor complexed to Rabaptin-5 links nucleotide exchange to effector recruitment and function. *Cell* **90**, 1149-1159.

Huttlin, E. L., Bruckner, R. J., Paulo, J. A., Cannon, J. R., Ting, L., Baltier, K., Colby, G., Gebreab, F., Gygi, M. P., Parzen, H. et al. (2017). Architecture of the human interactome defines protein communities and disease networks. *Nature* **545**, 505-509.

Ikeda, Y., Kawai, K., Ikawa, A., Kawamoto, K., Egami, Y. and Araki, N. (2017). Rac1 switching at the right time and location is essential for Fcγ receptor-mediated phagosome formation. *J. Cell Sci.* **130**, 2530-2540.

Jones, D. R., Foulger, R., Keune, W.-J., Bultsma, Y. and Divecha, N. (2013). PtdIns5P is an oxidative stress-induced second messenger that regulates PKB activation. *FASEB J.* **27**, 1644-1656.

Kubo, H., Hazeki, K., Takasuga, S. and Hazeki, O. (2005). Specific role for p85/p110beta in GTP-binding-protein-mediated activation of Akt. *Biochem. J.* **392**, 607-614.

Lu, Q., Yu, J., Yan, J., Wei, Z. and Zhang, M. (2011). Structural basis of the myosin X $PH1_N$-PH2-$PH1_C$ tandem as a specific and acute cellular $PI(3,4,5)P_3$ sensor. *Mol. Biol. Cell* **22**, 4268-4278.

Mao, Y. S., Yamaga, M., Zhu, X., Wei, Y., Sun, H.-Q., Wang, J., Yun, M., Wang, Y., Di Paolo, G., Bennett, M. et al. (2009). Essential and unique roles of PIP5K-gamma and -alpha in Fcgamma receptor-mediated phagocytosis. *J. Cell Biol.* **184**, 281-296.

Niebuhr, K., Giuriato, S., Pedron, T., Philpott, D. J., Gaits, F., Sable, J., Sheetz, M. P., Parsot, C., Sansonetti, P. J. and Payrastre, B. (2002). Conversion of $PtdIns(4,5)P_2$ into PtdIns(5)P by the *S.flexneri* effector IpgD reorganizes host cell morphology. *EMBO J.* **21**, 5069-5078.

Ninomiya, N., Hazeki, K., Fukui, Y., Seya, T., Okada, T., Hazeki, O. and Ui, M. (1994). Involvement of phosphatidylinositol 3-kinase in Fc gamma receptor signaling. *J. Biol. Chem.* **269**, 22732-22737.

Ramel, D., Lagarrigue, F., Pons, V., Mounier, J., Dupuis-Coronas, S., Chicanne, G., Sansonetti, P. J., Gaits-Iacovoni, F., Tronchère, H. and Payrastre, B. (2011). Shigella flexneri infection generates the lipid PI5P to alter endocytosis and prevent termination of EGFR signaling. *Sci. Signal.* **4**, ra61.

Riedl, J., Crevenna, A. H., Kessenbrock, K., Yu, J. H., Neukirchen, D., Bista, M., Bradke, F., Jenne, D., Holak, T. A., Werb, Z. et al. (2008). Lifeact: a versatile marker to visualize F-actin. *Nat. Methods* **5**, 605-607.

Sbrissa, D., Ikonomov, O. C., Deeb, R. and Shisheva, A. (2002). Phosphatidylinositol 5-phosphate biosynthesis is linked to PIKfyve and is involved in osmotic response pathway in mammalian cells. *J. Biol. Chem.* **277**, 47276-47284.

Schlam, D., Bagshaw, R. D., Freeman, S. A., Collins, R. F., Pawson, T., Fairn, G. D. and Grinstein, S. (2015). Phosphoinositide 3-kinase enables phagocytosis of large particles by terminating actin assembly through Rac/Cdc42 GTPase-activating proteins. *Nat. Commun.* **6**, 8623.

Segawa, T., Hazeki, K., Nigorikawa, K., Morioka, S., Guo, Y., Takasuga, S., Asanuma, K. and Hazeki, O. (2014). Inpp5e increases the Rab5 association and phosphatidylinositol 3-phosphate accumulation at the phagosome through an interaction with Rab20. *Biochem. J.* **464**, 365-375.

Segawa, T., Hazeki, K., Nigorikawa, K., Nukuda, A., Tanizawa, T., Miyamoto, K., Morioka, S. and Hazeki, O. (2017). Inhibitory receptor FcγRIIb mediates the effects of IgG on a phagosome acidification and a sequential dephosphorylation system comprising SHIPs and Inpp4a. *Innate Immun.* **23**, 401-409.

Szymańska, E., Sobota, A., Czuryło, E. and Kwiatkowska, K. (2008). Expression of $PI(4,5)P_2$-binding proteins lowers the $PI(4,5)P_2$ level and inhibits FcgammaRIIA-mediated cell spreading and phagocytosis. *Eur. J. Immunol.* **38**, 260-272.

Tuosto, L., Capuano, C., Muscolini, M., Santoni, A. and Galandrini, R. (2015). The multifaceted role of PIP2 in leukocyte biology. *Cell. Mol. Life Sci.* **72**, 4461-4474.

Ungewickell, A., Hugge, C., Kisseleva, M., Chang, S.-C., Zou, J., Feng, Y., Galyov, E. E., Wilson, M. and Majerus, P. W. (2005). The identification and characterization of two phosphatidylinositol-4,5-bisphosphate 4-phosphatases. *Proc. Natl. Acad. Sci. USA* **102**, 18854-18859.

Viaud, J., Lagarrigue, F., Ramel, D., Allart, S., Chicanne, G., Ceccato, L., Courilleau, D., Xuereb, J.-M., Pertz, O., Payrastre, B. et al. (2014). Phosphatidylinositol 5-phosphate regulates invasion through binding and activation of Tiam1. *Nat. Commun.* **5**, 4080.

Vicinanza, M., Korolchuk, V. I., Ashkenazi, A., Puri, C., Menzies, F. M., Clarke, J. H. and Rubinsztein, D. C. (2015). PI(5)P regulates autophagosome biogenesis. *Mol. Cell* **57**, 219-234.

Vieira, O. V., Bucci, C., Harrison, R. E., Trimble, W. S., Lanzetti, L., Gruenberg, J., Schreiber, A. D., Stahl, P. D. and Grinstein, S. (2003). Modulation of Rab5 and Rab7 recruitment to phagosomes by phosphatidylinositol 3-kinase. *Mol. Cell. Biol.* **23**, 2501-2514.

Zou, J., Marjanovic, J., Kisseleva, M. V., Wilson, M. and Majerus, P. W. (2007). Type I phosphatidylinositol-4,5-bisphosphate 4-phosphatase regulates stress-induced apoptosis. *Proc. Natl. Acad. Sci. USA* **104**, 16834-16839.

Supplemental Tables

Table SI. Target sequences for shRNA

TMEM55a 229	5'-GTGCACAGTTTGCAATGAA-3'
TMEM55a 322	5'-GGATACATCTCGGCGAATA-3'
TMEM55b 384	5'-GCATCAGCATGTAGTCAAA-3'

Table SII. Primers for RT-PCR

TMEM55a (F)	5'-CGGGAAATGTCACTCCCACA-3'
TMEM55a (R)	5'-CFFGTTCCTGGACTGGCGAT-3'
TMEM55b (F)	5'-CCGCCCCAGGCATTTCC-3'
TMEM55a (R)	5'-TATCCGGGCTAGTCAAGGGT-3'

Table SIII. Primers for silent mutagenesis for the add back

TMEM55a (F)	5'-GGTTAAGTGCACCGTGTGCAATGAAGCTAC-3'
TMEM55a (R)	5'-GTAGCTTCATTGCACACGGTGCACTTAACC-3'

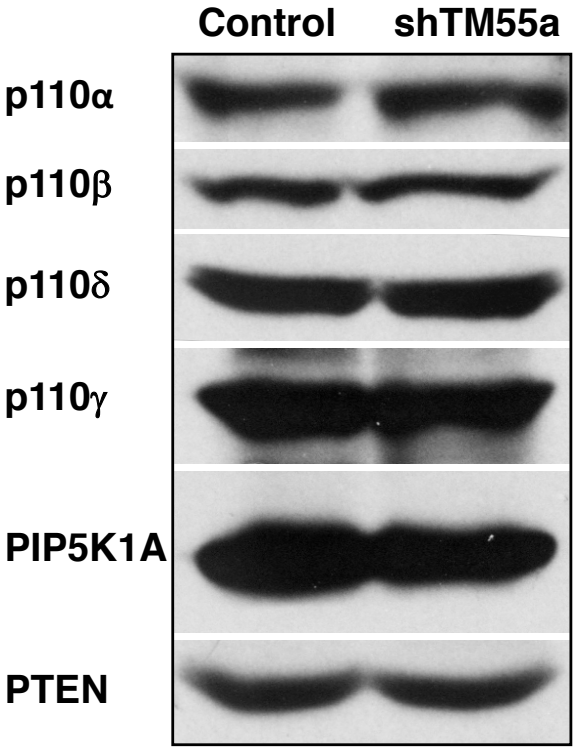

Fig. S1. Protein expression of enzymes that involved in PtdIns(4,5)P2 and PtdIns(3,4,5)P3 metabolism. Cell lysates prepared from control and TMEM55a-deficient cells were analyzed by Western blotting.

The antibodies used were:

p110α BD #611398

p110β sc (S-19)

p110δ BD #611014

p110γ sc (N-16)

PIP5K1A GTX#111953

PTEN Cell Signaling #9552

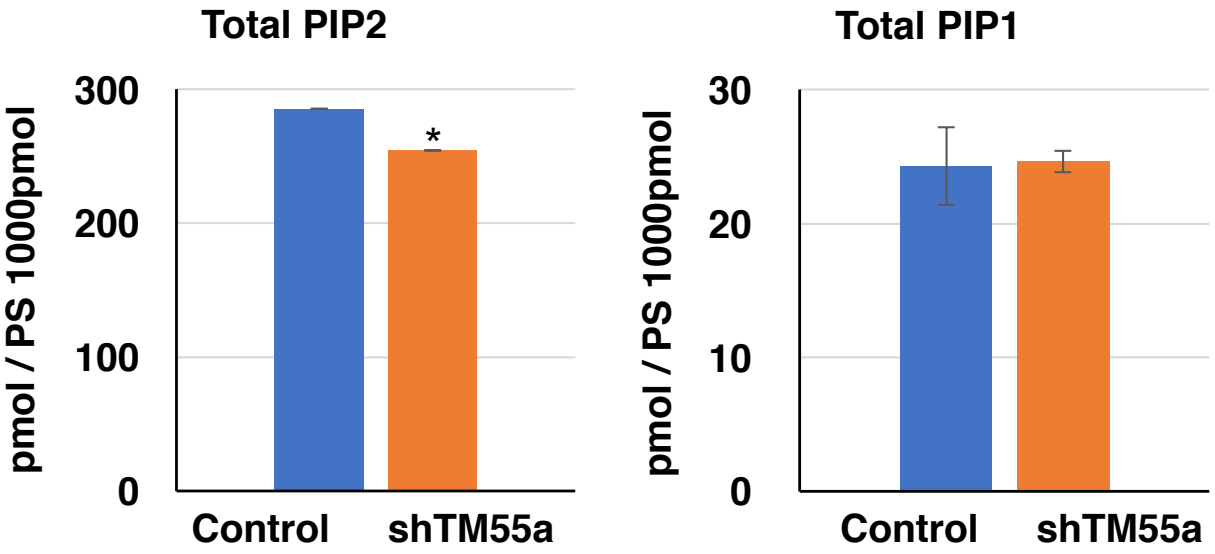

Fig. S2. Phosphoinositide Measurement
For PtdIns measurement, acidic phospholipids were extracted from control and shTMEM55a cells by the Bligh–Dyer method. An UltiMate 3000 LC system (Thermo Fisher Scientific) equipped with HTC PAL autosampler (CTC Analytics) was used for column chromatography. TSQ-Vantage (Thermo Fisher Scientific) was used for electrospray ionization MS/MS analysis. (Kofuji S. et al. (2015). INPP4B Is a PtdIns(3,4,5)P_3 Phosphatase That Can Act as a Tumor Suppressor. *Cancer Discov* **5**, 730–9)